


Article

ZIF-67 Derived MnO₂ Doped Electrocatalyst for Oxygen Reduction Reaction

Usman Salahuddin ^{1,2}, Naseem Iqbal ^{1,*} , Tayyaba Noor ³, Saadia Hanif ¹, Haider Ejaz ¹, Neelam Zaman ¹ and Safeer Ahmed ⁴

¹ U.S.-Pakistan Center for Advanced Studies in Energy (USPCASE), National University of Sciences and Technology, Islamabad 44000, Pakistan; usmanscme@gmail.com (U.S.); saadiah_hanif@yahoo.com (S.H.); haider@uspcase.nust.edu.pk (H.E.); neelamzaman6650@gmail.com (N.Z.)

² Institute of Material Science, University of Connecticut, Storrs, CT 06268, USA

³ School of Chemical and Materials Engineering (SCME), National University of Sciences and Technology, Islamabad 44000, Pakistan; tayyaba.noor@scme.nust.edu.pk

⁴ Department of Physical Chemistry, Quaid-e-Azam University, Islamabad 45320, Pakistan; safeerad@qau.edu.pk

* Correspondence: naseem@uspcase.nust.edu.pk

Abstract: In this study, zeolitic imidazolate framework (ZIF-67) derived nano-porous carbon structures that were further hybridized with MnO₂ were tested for oxygen reduction reaction (ORR) as cathode material for fuel cells. The prepared electrocatalyst was characterized by X-ray powder diffraction (XRD), scanning electron microscopy (SEM) and Energy Dispersive X-ray Analysis (EDX). Cyclic voltammetry was performed on these materials at different scan rates under dissolved oxygen in basic media (0.1 M KOH), inert and oxygen rich conditions to obtain their I–V curves. Electrochemical impedance spectroscopy (EIS) and Chronoamperometry was also performed to observe the materials' impedance and stability. We report improved performance of hybridized catalyst for ORR based on cyclic voltammetry and EIS results, which show that it can be a potential candidate for fuel cell applications.

Keywords: fuel cell; oxygen reduction reaction (ORR); metal organic frameworks (MOFs)



Citation: Salahuddin, U.; Iqbal, N.; Noor, T.; Hanif, S.; Ejaz, H.; Zaman, N.; Ahmed, S. ZIF-67 Derived MnO₂ Doped Electrocatalyst for Oxygen Reduction Reaction. *Catalysts* **2021**, *11*, 92. <https://doi.org/10.3390/catal11010092>

Received: 9 December 2020

Accepted: 5 January 2021

Published: 12 January 2021

Publisher's Note: MDPI stays neutral with regard to jurisdictional claims in published maps and institutional affiliations.



Copyright: © 2021 by the authors. Licensee MDPI, Basel, Switzerland. This article is an open access article distributed under the terms and conditions of the Creative Commons Attribution (CC BY) license (<https://creativecommons.org/licenses/by/4.0/>).

1. Introduction

Consumption and production of energy is the sign of industrial growth and progress of any country, as energy develops everything, and around 85% of our energy commitments depend upon fossil fuels [1,2]. However, energy resources such as fossil fuels reduce speedily due to escalating life standards and growing populations. In addition, the economic growth of developed countries, industrial civilization and modern lifestyles rely on the energy withdrawal from gas and oil supplies [3,4]. For intermittent energy generation technologies to strengthen their foothold, energy storage solutions need to become better performing and economically viable [5].

Recently, fuel cells have been considered to be a promising energy resource in contrast to other substitutes that convert chemical energy into electrical energy during a catalytic reaction [6,7]. Various types of fuel cells are available among these; the polymer electrolyte membrane fuel cell (PEMFC) and alkaline fuel cell (AFC) have the advantage of having smaller size, light weight and astonishing power density [8]. Consequently, they can be utilized for stationary and portable applications. They can perform work constantly at low temperature and give high current densities [9]. Cost and stability, however, are the two main factors that delay the commercialization of fuel cells at a large scale.

Since the key cost is because of extreme and ineffective utilization of platinum based electro catalysts, Pt electrodes present the ideal catalytic activity for ORR (oxygen reduction reaction), thus serving as a standard electrode for all the catalysts prepared up until

now [10]. Time is needed to prepare various new non-noble metal catalysts which have generated a lot of attraction because of their vastly effectual catalytic properties [11,12].

Multiple techniques have been tested to address the catalysis, including the use of microspheres, nanoparticles, perovskites, etc., of which metal organic frameworks are also part [13–17]. Recently, metal organic frameworks (made up of organic ligands and Inorganic metal ions) have been the subject of significant attention in the field of electrochemistry because they have a variety of structures with large surface area, large pore volume, high porosity and tunable pore size, and are being tested as an economically viable substitutes for noble metal nano-composites [18,19]. Wang et. al. designed a carbon matrix with nitrogen phosphorous doping using Cu-MOF, showing an extraordinary performance as an electro-catalyst for hydrogen evolution reaction (HER) and ORR [20].

In addition, the nano sized pores present in the metal organic frameworks, when turned into porous carbons, make the access to guest molecules much easier, thus increasing the likelihood of an active site being available [21]. Moreover, nano carbons formed from metal organic frameworks are formed as sheets, nanotubes and multiple other forms which can act as high-performance nonmetal catalysts. Besides, for improving their mechanical strength and conductivity, they are transformed conventionally into NPC (nitrogen doped nanoporous carbon), which has shown outstanding performance in the electrochemical field. Gai et al. modify an electrode by NPC prepared from ZIF-8 for the detection of uric acid, ascorbic acid and dopamine. Rizvi et.al. reported Cu-MOF Derived Cu@AC electrocatalyst for ORR in PEMFC. The composite Cu@AC (1:1) shows the peak current density of 2.11 mA cm^{-2} in 0.1 M KOH at a potential of 0.9 V with a scan rate of 50 mV s^{-1} , which shows superior activity compared to commercial grade Pt/C, having a peak current density of 1.37 mA cm^{-2} at a potential of 0.86 V [10]. Moreover, bimetallic MOFs have been utilized to boost the catalyst electrocatalytic performance [22,23]. Yoon et al. reported new bimetallic 2D MOFs ($\text{Co}_x\text{Ni}_y\text{-CATs}$) for electrochemical reduction of oxygen; the two metal ions, i.e., Co^{2+} and Ni^{2+} , are rationally controlled in $\text{Co}_x\text{Ni}_y\text{-CATs}$ (a bimetallic catalyst) for efficient performance in the oxygen reduction reaction (ORR) [24].

Electro catalysts derived from metal organic frameworks, i.e., ZIFs (Zeolitic imidazole frameworks), which are rich in transition metals, i.e., Zn^{+2} , CO^{+2} and nitrogen and carbon and preparation of Zeolitic frameworks, which are single-site solid catalysts with effective and uniform catalytic activity, can be accomplished via the use of metal organic frameworks [25,26]. The metal organic framework is a nitrogen and carbon precursor with a transition metal and is heat treated at 800–1000 °C to form nitrogen doped electro catalyst [27]. ZIFs have been utilized in the production of ORR catalysts where a metal–nitrogen–carbon structure is formed when ZIF-67 is pyrolyzed in the presence of iron carrier, which showed effective electrochemical activity owing partially to the increased surface area provided to the active metals [28,29]. ZIF-67 can also provide the basis for creating tunable structures owing to the ordered arrangement of atoms in the framework. The formation of nanocrystals of carbon decorated with cobalt catalyst has been reported with the ability to catalyze ORR and to perform this function in symmetry. Cobalt containing ZIF-67 based catalysts can also perform catalysis under special preparatory conditions [30,31]. This ability to create uniform crystals can also be utilized in conjunction with the flexibility of carbon materials for ORR [32,33].

Besides cobalt and nickel, manganese has also been shown to perform catalytic activity pertaining to oxygen reduction, which has sparked interest in utilizing this capability in ZIF-67 based carbon electrodes [34,35]. Work with ZIF-67 involving the use of magnesium oxides has yielded remarkable enhancement in the catalytic capability of carbon-based electrodes. In work utilizing Mn_3O_4 and Co_3O_4 , aimed at catalyzing water splitting reactions and oxygen reduction, the reversible overpotentials were reported to be better than those shown by electrodes containing noble metals like platinum and ruthenium [36,37].

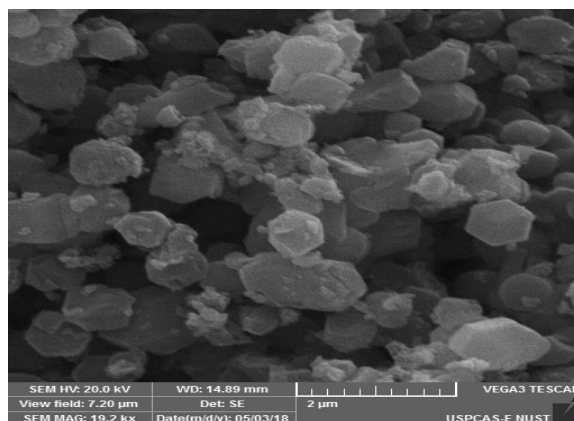
In this paper, we have followed a novel approach to recommend a new material for ORR reaction in fuel cells. ZIF-67 derived nanoporous carbon was modified with MnO_2 particles using a simple hydrothermal process to enhance its ORR performance. Both

ZIF-67 derived nanoporous carbon and the modified sample were tested through cyclic voltammetry to analyze the difference in their individual performance.

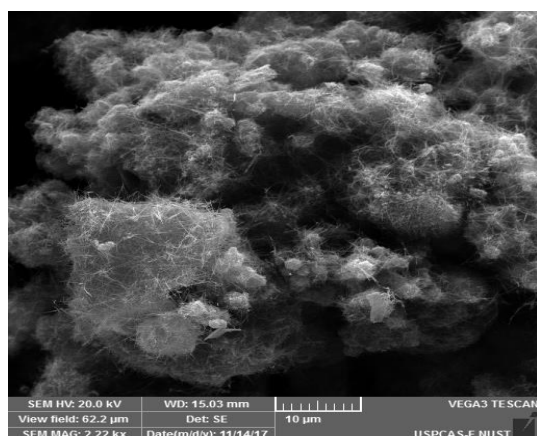
2. Results and Discussion

2.1. Characterization of Prepared Catalyst

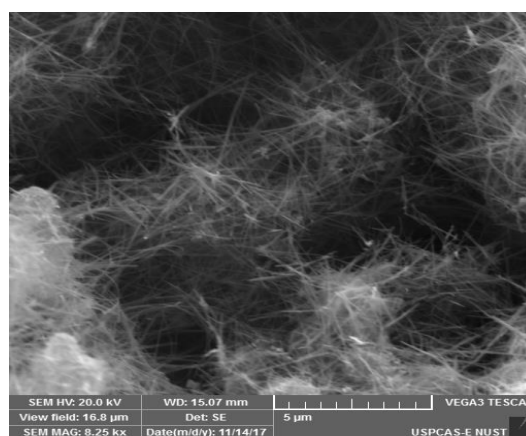
The morphology of synthesized catalysts such as ZIF-67, ZIF derived carbon nanotubes (ZCNT) and Manganese oxide doped ZCNT (ZCNT-M) was analyzed by scanning electron microscopy as illustrated in Figure 1a–c. The rhombic dodecahedron shaped nano crystal of the ZIF-67 is well preserved, as shown in Figure 1a.



(a)



(b)



(c)

Figure 1. SEM images of (a) ZIF-67, (b) ZCNT and (c) ZCNT-M.

From Figure 1b,c, it was observed that after pyrolysis of ZIF-67, carbon nanotubes (CNTs) are visible in SEM images of ZCNT and ZCNT-M. Moreover, at high magnification, the SEM image shows that the obtained ZIF-67 surface was smooth, and their dodecahedron-shaped crystals were closely affixed to the CNTs. In addition, the surface pop and shacks of ZIF-67 nanoparticles more evidently approve that nanoparticles of ZIF-67 were in situ grown on CNTs' surfaces.

The EDS analysis of prepared catalysts such as ZCNT and ZCNT-M shows the presence of manganese, cobalt, oxygen and carbon without any impurity. Table 1 shows the weight percentages of the following element. ZCNT has the maximum carbon percentage while other samples such as ZCNT-M have comparatively lower percentages of carbon, as the unstable organic groups have evaporated after heating, which also reduces the carbon percentage. Moreover, after Mn loading, the relative wt. % of carbon decreases in ZCNT-M, correspondingly.

Table 1. EDS outcome of ZCNT, ZCNT-M.

Sample Element	ZCNT	ZCNT-M
C wt %	50.02	15.98
O wt %	19.07	47.91
Co wt%	30.91	9.99
Mn wt%	-	24.80

Moreover, EDS elemental mapping images, i.e., Figure 2a,b, illustrate that the uniform loading of Mn in the sample and the elemental composition match well with the expected ratio of elemental weight and atomic %.

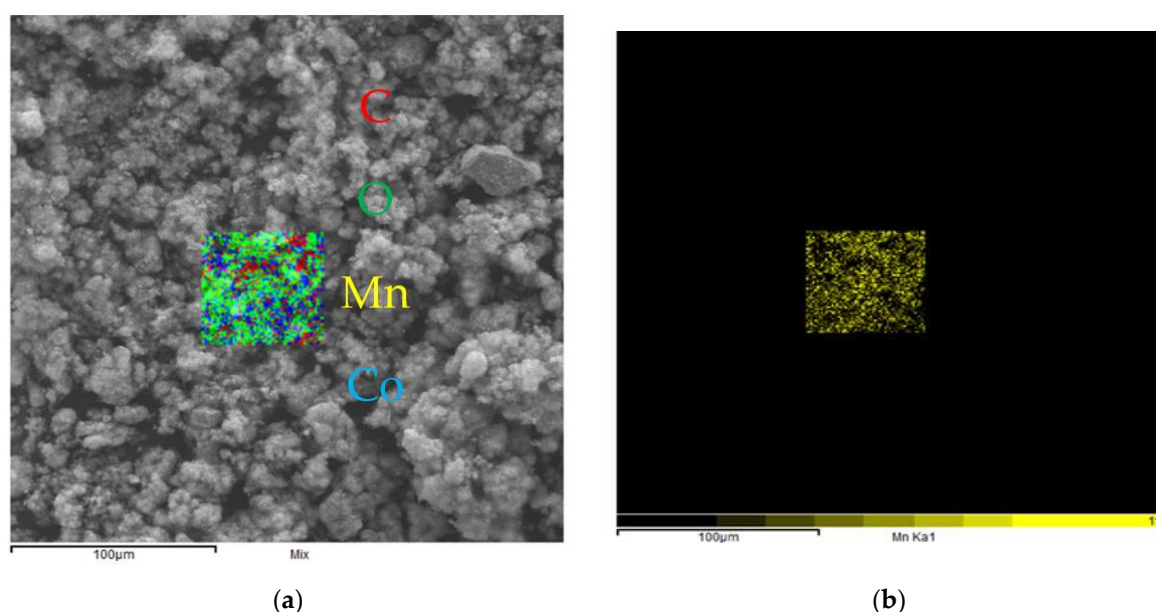
**Figure 2.** Elemental Mapping of ZCNT-M. (a) map showing C, O, Mn & Co distribution, (b) map showing Mn distribution.

Figure 3a illustrates the XRD pattern of ZIF-67. The presence of characteristic peaks indicates the successful synthesis of material, i.e., 7.2° (011), 10.4° (002), 12.7° (112), 14.7° (022), 16.4° (013), 18° (222), 22.1° (114), 26.5° (134), 29.6° (044), 31.3° (244), 32.5° (235), and 43.1° (100) [38].

Figure 3b illustrates the XRD pattern of prepared ZCNT. The peak at 26.3° (002) confirms the presence of graphitized CNTs and other peaks at 44.36° , 51.67° and 75.98° correspond to Co (111), Co (200) and Co (220) [39].

Figure 3c illustrates the XRD pattern of prepared ZCNT-M sample. The presence of characteristic peaks corresponds to cobalt carbide (JCPDS card number 43-1144) [40], cobalt oxide (JCPDS card number 43-1003) [41], manganese oxide (JCPDS card number 44-0141) [42] and cobalt manganese oxide (JCPDS card number 32-0297) [43].

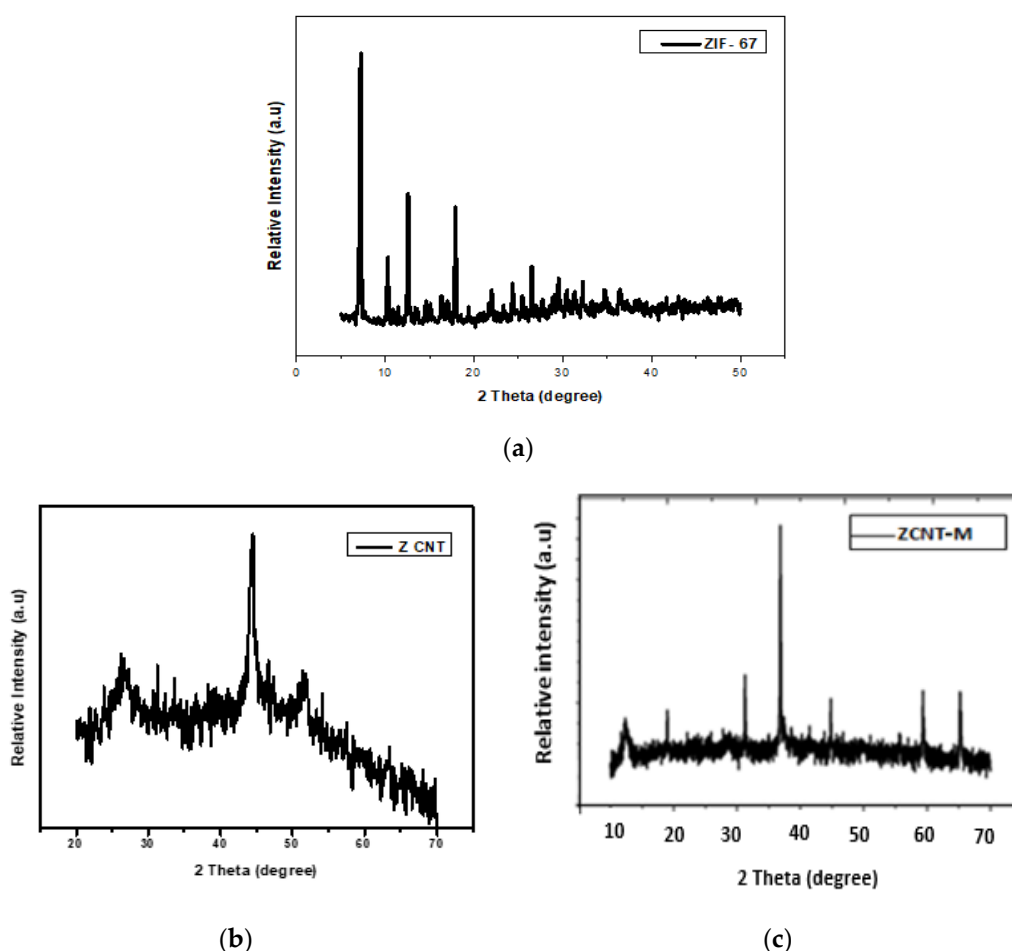


Figure 3. XRD plot for (a) ZIF-67 (b) ZCNT (c) ZCNT-M.

2.2. Electrochemical Analyses

Eco Chemie Autolab PGSTAT 302 potentiostat/galvanostat (Utrecht, The Netherlands) was used to perform cyclic voltammetry measurements and GPES software 4.9 was used to run the experiments on the equipment. A three-electrode system was used in which Ag/AgCl was used as the reference electrode, platinum wire as the counter electrode, while glassy carbon (7.065 mm²) was used as the working electrode.

Moreover, for the modification of working electrode (GCE) ink is deposited on its surface and ink is prepared by adding ZCNT and ZCNT-M catalyst in 100 μ L ethanol with 20 μ L Nafion (5 wt %) as the binding and conducting agent to form the catalyst ink, which was later deposited (20 μ L) on the glassy carbon electrode and allowed to dry. All the prepared composites were tested for different techniques, i.e., cyclic voltammetry, chronoamperometry and electrochemical impedance spectroscopy (EIS) in 0.1 M KOH (an electrolyte) by using the same method of preparing ink. In addition, ZCNT and ZCNT-M samples were tested under inert, dissolved oxygen and oxygen rich conditions. A frequency range of 10 to 40 kHz with a scan rate amplitude of 50 mVs^{−1} was used for electrochemical impedance spectroscopy under potentiostatic mode. Chronoamperometry was also performed for 3600 s.

2.3. Electrochemical Evaluation of Prepared Catalysts

At first, ZIF-67 derived CNTs (ZCNT) and ZIF-67 derived CNTs/MnO₂ (ZCNT-M) were compared. To ensure that dissolved oxygen is the only analyte present within the KOH solution and there are no other analyte species to react with the electrode, the solution was purged with argon gas for 2–3 min and then the response was recorded and compared with

oxygen dissolved solution. Figure 4 shows that in the presence of oxygen, the prepared catalysts' reduction current was noticeably increased, which may be attributed to the presence of continuously regenerated reaction centers that might lead to current value amplification during the reduction process [44].

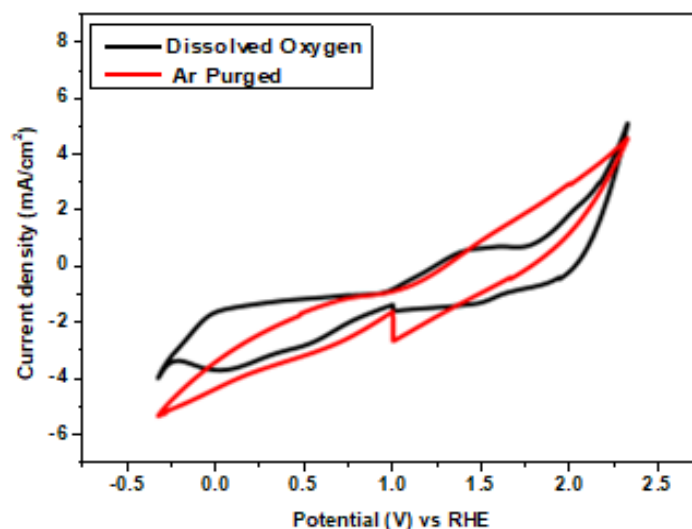


Figure 4. ZCNT-M Performance under dissolved O_2 and Ar purged environment.

With an optimal flow rate of oxygen gas and at a scan rate of 50 mV/s, cyclic voltammetry of prepared catalysts was performed; in this study, the electrochemical activity of ZCNT was compared with ZCNT-M to obtain the values of peak current density, onset potential and peak potentials for oxygen reduction reactions, as illustrated in Figure 5. From the figure, it can be observed that ORR performance of ZCNT-M is much better than ZCNT due to the addition of MnO_2 , and it has markedly increased the current densities up to 6.56 mA/cm² for ORR with an ORR onset potential (V vs. RHE) of 1.02 V, which is comparable with that of Pt/C (1.01 V), illustrating that there is a current density of 5.02 mA/cm² [45]. In comparison to ZCNT-M, commercial MnO_2 shows remarkably low current density with 0.25 mA/cm² and with onset potential (V vs. RHE) of 0.96 V, as reported by Huang et al. and Chhetri et al. [46,47]. The increased current densities of ZCNT-M can be attributed to good catalytic ORR activity of MnO_2 ; as with the ZIF-67 derived CNTs (ZCNT), it enhances the surface area and conductivity of prepared catalysts to a significant level. Thus, as-prepared ZCNT-M composite was used as an efficient non-precious cathodic electrocatalyst with preferable ORR stability, enhanced electron-transport performance, and elevated antitoxic property in alkaline media for ORR.

Figure 6 illustrates the effect of scan rate on the current density of the prepared sample. All the tests were executed with a diverse range of scan rate values such as 5 mV/s, 15 mV/s, 25 mV/s and 50 mV/s in an alkaline media (0.1 M KOH). Prepared ink composition (i.e., 3 mg per catalyst) remained the same in all the experiments. The current density of ZCNT-M in 0.1M KOH for ORR increased gradually because of electroactive species' easy access to the surface of the electrode in the less time period [5]; also, at high scan rates, non-electrolytic species were not able to be reduced or oxidized into products. Consequently, only electroactive products were liable for high current density values, this remarkable response of catalyst is linked to the improved extent of reaction. Moreover, a slight shift in peaks was observed, which indicated a slight irreversibility during reaction.

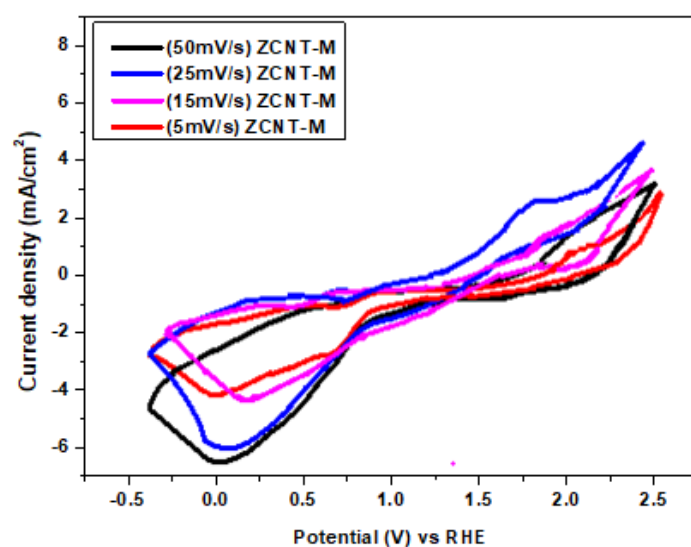


Figure 5. Cyclic voltammograms of ZCNT and ZCNT-M for ORR.

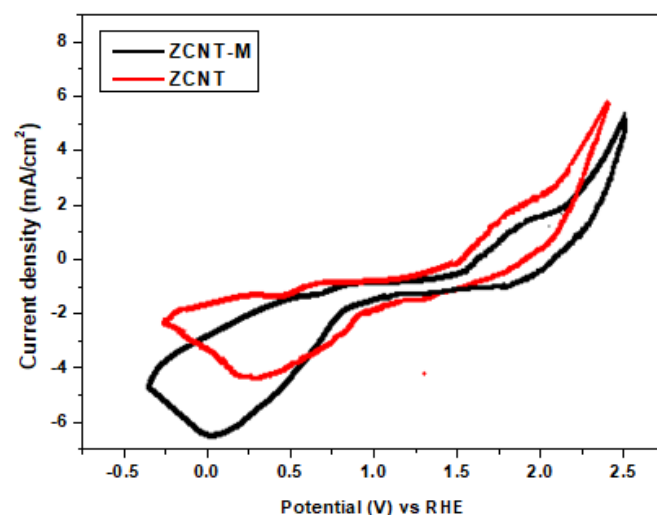


Figure 6. Cyclic voltammograms at different scan rates for ZCNT-M.

Furthermore, linear sweep voltammetry was performed with oxygen purging to study the effect of increasing analyte concentration on current density, as shown in Figure 7. Pure oxygen was purged through the electrolyte for one, two and three minutes, respectively, before performing the linear cyclic voltammetry experiment. A continuous supply of oxygen was maintained during the experimental run. Oxygen purging showed a marked increase in the current density relative to the dissolved oxygen case for ORR. The graph below shows that peak current densities increased as the amount of oxygen present in the electrolyte was increased; however, the current density decreased beyond two minutes of oxygen purging. A possible explanation for this decrease is the saturation of the electrolyte with analyte along with a decrease in oxygen diffusion to the electrode surface.

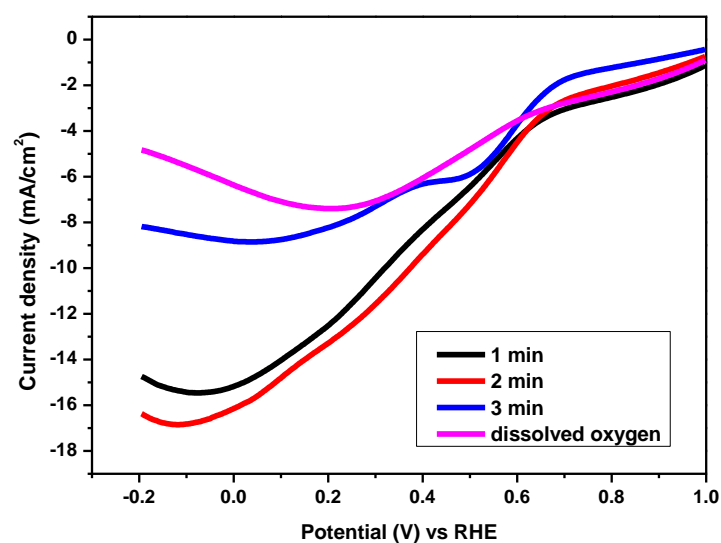


Figure 7. Current densities at different oxygen purging durations for ZCNT-M.

Furthermore, the kinetics of ORR reactions were found to be diffusion controlled. A plot between the square root of scan rate and peak current density was made for ZCNT-M, as shown in Figure 8.

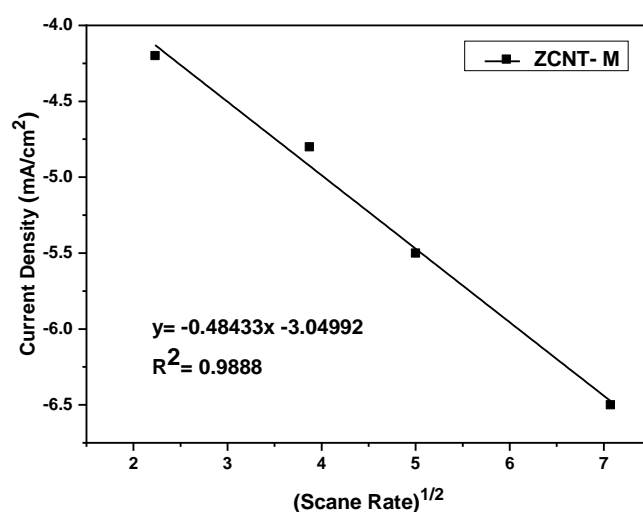


Figure 8. Scan rate vs. peak current density for ZCNT-M.

The figure illustrates that the square roots of scan rates and current densities have a linear relationship, while this linear plot is relative to $D^{1/2}$ to obtain the slope value. Moreover, diffusion coefficients were calculated using the Randles-Sevcik Equation (1) [48].

$$I_p = 0.4463nFAC\sqrt{\frac{nFvD}{RT}} \quad (1)$$

where D is the diffusion coefficient, A is the active surface area (cm^2), C is the molar bulk concentration of 0.1 M KOH, v is the scan rate (V s^{-1}), and n is the number of electrons transferred.

The diffusion coefficients for ORR of ZCNT-M are calculated as $D_{\text{ORR}} = 6.6 \times 10^{-4} \text{ cm}^2/\text{s}$. These results support that a diffusion-controlled mechanism is followed by electrocatalytic oxygen evaluation reaction and oxidation reduction reaction.

Finally, to analyze the trend of overpotential with the current density, Tafel plots (Figure 9) were made which were then used to calculate the exchange current densities

value of $1.49 \times 10^{-3} \text{ A/cm}^2$. Firstly, overpotential is calculated by using the formula such as $E - E_0$ [19]. In order to comprehend the reaction kinetic performance, Tafel slopes were calculated by using the subsequent Equation (2).

$$d\eta/d \ln |j| = -RT/\alpha nF \quad (2)$$

where α was calculated by using Equation (3) [42]:

$$E_p - E_p/2 = 1.857 RT/\alpha F \quad (3)$$

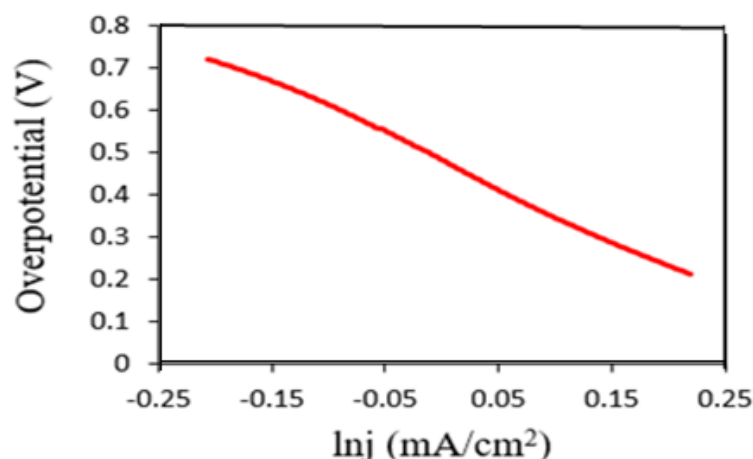


Figure 9. Tafel plots for ZCNT-M.

For the oxygen reduction reaction, n was deemed to be 4. The Tafel slope value for ZCNT-M is calculated and obtained in the range of 165–200 mV/dec, and the value of slope is determined such that if $>118 \text{ mV/dec}$, then the rate determining steps are ascribed via (i) ongoing chemical oxidation, (ii) the resulting chemical combination and (iii) the transfer of electrons occurring via an oxide layer. In order to elude the confusion, the outcomes collected from the Tafel slopes will be referred as “cathodic quantities” and the mechanisms for ORR can be established precisely by these approaches [17]. The outcomes are in accord with the literature, where the first C–H bond breaking in ORR occurs because of the low potential region along with the rate determining step through the first electron transfer, while in the high potential region, the increase in slope values is because of poisonous intermediate species having less exposure [10].

To understand the activity of the modified electrode in a better way, electrochemical impedance spectroscopy was performed using the same three electrode systems in 0.1 M KOH solution under the potentiostatic mode. The Nyquist plot below in Figure 10 represents two regions, presenting an idea regarding solution resistance (R_s) and charge transfer resistance (R_{ct}); the small semicircle clearly shows that the charge transfer resistance for ZCNT-M is lower in comparison to ZCNT. Moreover, corresponding low R_{ct} and R_s values are liable for higher catalyst activity as well [5,49]. The decreased value of resistance in ZCNT-M can be attributed in good catalytic ORR activity of MnO_2 , as it improves the surface area and conductivity of prepared catalysts to a significant level. Similarly, the high electronic and ionic conductivity of ZCNT-M may possibly be responsible for the straight line. This significant reduction in charge transfer resistance in ZCNT-M clearly favors ORR reactions in ZCNT-M as compared to ZCNT.

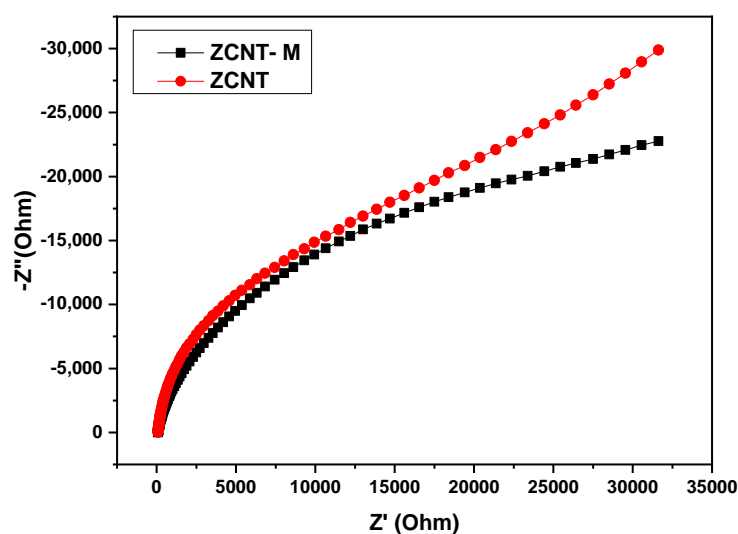


Figure 10. Electrochemical impedance spectroscopy (EIS) plot for ZCNT-M and ZCNT.

The prepared catalysts' stability was determined via the chronoamperometry technique, a key parameter to accomplish the practical application of synthesized samples. The stability test of ZCNT-M was carried out in 0.1 M KOH solution at a potential of 0.1 V for 3600 s in the similar three electrode setup and subsequent electrolyte. At the start, the current dropped substantially very quickly, which can be justified with the following reasons: (a) adsorption of reaction intermediate to the electrode surface; (b) blockage of active site due to evolved oxygen accumulation on the surface of the electrode [10] and (c) flake off material caused by extreme bubbling, but later it adopted a fairly stable trend for the remainder of the hour, as shown in the Figure 11 below. Moreover, Figure 12 shows the plot between the current and square root of current and describes a linear trend over time.

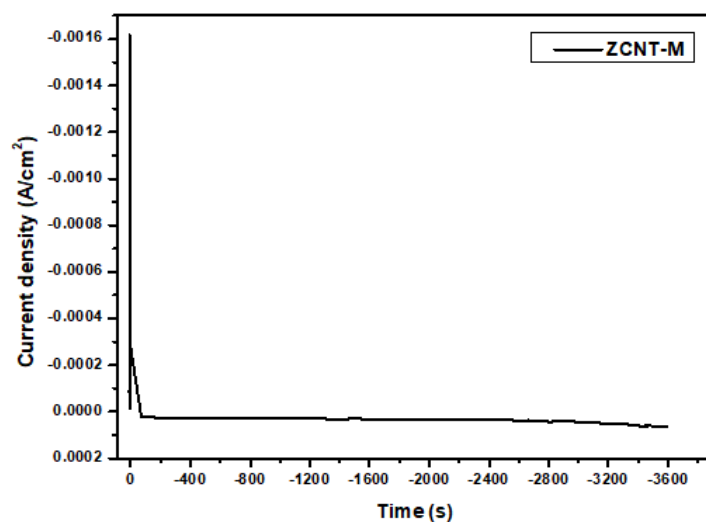


Figure 11. Chronoamperometric plot for ZCNT-M.

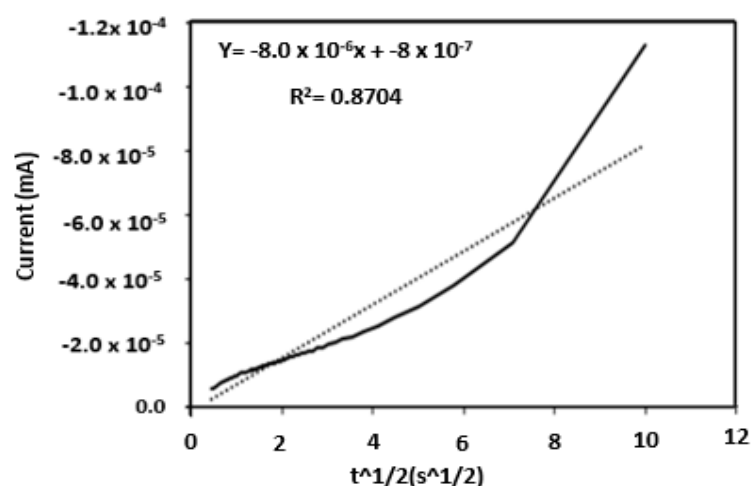


Figure 12. Chronoamperometric plot between current and square root of current for ZCNT-M.

Figure 13 shows the mechanism of ORR in basic media (KOH); it describes the complex reaction pathway by which reductive splitting of the oxygen O–O bond occurs on the catalyst adsorbed surface. Here, k_1 epitomizes the direct reduction of O_2 to OH^- ion without any intermediate formation.

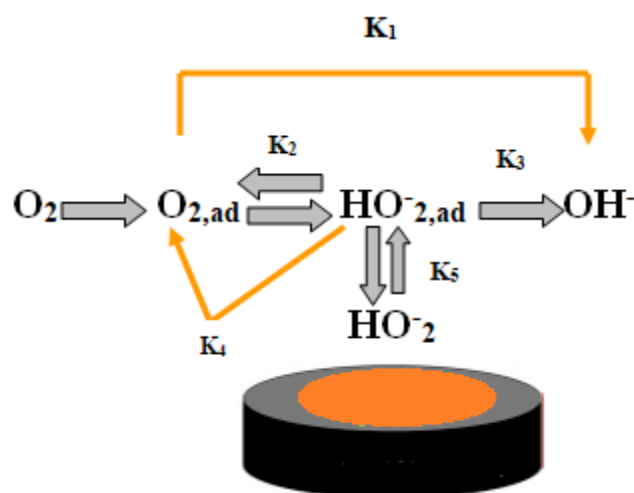


Figure 13. Oxygen reduction reactions (ORR) mechanism on the surface of electrode.

In addition, the k_2 is a comprehensive rate constant for the adsorbed peroxide formation, and might implicate other rate constants that are associated to both the disproportionation reaction and intermediate formation of the adsorbed super oxide; besides, k_3 is the rate constant for peroxide reduction, k_4 refers to the catalytic decaying of adsorbed peroxide on the electrode surface, and k_5 represents rate constants for peroxide desorption and adsorption processes [50].

3. Experimental

3.1. Characterization

To study the surface morphologies of prepared catalysts, SEM analysis was conducted with VEGA3 TESCON at the voltage of 20 kV. For elemental analysis of prepared catalysts, EDS analysis was conducted. Moreover, the crystal structure and phase purity of the prepared catalyst was established by XRD analysis (D8 Advanced Diffractometer) by using Jade 6.0 with diffraction angle (2θ), at a range of $10\text{--}70^\circ$, with the step size of $4^\circ/\text{s}$.

3.2. Synthesis of ZIF-67

A quantity of 1.97 g of 2-methylimidazole was dissolved in a 40 mL of 50/50 (v/v %) of ethanol and methanol. Furthermore, 1.746 g of $\text{Co}(\text{NO}_3)_2 \cdot 6\text{H}_2\text{O}$ were mixed with ethanol and methanol mixture, keeping the ratios as before. The two solutions were then stirred together for 20 min and kept at room temperature for 20 h. After centrifugation, washing and drying, a purple precipitate was obtained [33].

3.3. Synthesis of Mesoporous Carbon

ZIF-67 was heated to 350 °C and was maintained at that temperature for 1.5 h using a tube furnace under reducing atmosphere (H_2/Ar). The temperature was then increased to 750 °C with a ramp rate of 2 °C/min and was sustained at that temperature for 3.5 h. The furnace was naturally allowed to cool down. The sample was then treated with H_2SO_4 , centrifuged, washed, and dried [51].

3.4. Synthesis of MnO_2 -Doped Mesoporous Carbon

Next, 1 M solution of KMnO_4 was prepared in deionized water. Nano-porous carbon particles derived from ZIF-67 were dispersed in the 100 mL of solution using a bath sonicator for 15 min. The mixture was then stirred for 30 min and HCl (30%) was added dropwise to the mixture. The mixture was then transferred into a Teflon lined autoclave and heated in a box furnace at 80 °C for 3 h. The heated suspension was then filtered and washed using ethanol/water mixture and eventually dried in a vacuum oven at 80 °C overnight. The dried sample is the desired product (ZIF-67 derived nano-porous carbon and MnO_2 hybrid). Figure 14 illustrates the synthesis route of ZCNT and ZCNT-M.

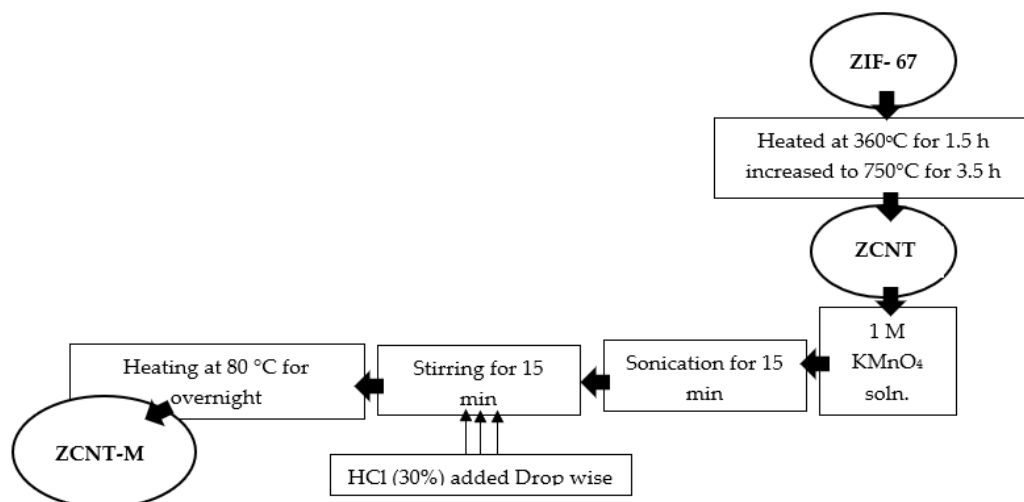


Figure 14. Synthesis route of ZCNT and ZCNT-M.

4. Conclusions

ZIF-67 derived nano-porous carbon that is further doped with MnO_2 particles offers a potential material to be used as ORR catalyst in fuel cells, and the material shows good ORR performance. Onset potentials, peak potential and peak current densities were calculated using current vs. voltage plots obtained through cyclic voltammetry. The modified material ZCNT-M showed better performance as compared to ZCNT, as observed through cyclic voltammetry and EIS. The material showed a performance enhancement up to a certain level of oxygen purging, as compared to its performance with dissolved oxygen in the electrolyte. In addition, electrochemical stability was tested by using chronoamperometry, showing a sudden decrease in current and stable performance up to 3600s. Ultimately, it can be concluded from this work that the good catalytic ORR activity of ZIF-67 derived CNTs/ MnO_2 (ZCNT-M) is due to the incorporation of MnO_2 not only enhancing the surface area, but also the conductivity of prepared catalysts to a significant level.

Author Contributions: Conceptualization, U.S.; Data curation, U.S., T.N., S.H., H.E. and N.Z.; Formal analysis, N.I., H.E. and S.A.; Investigation, T.N.; Methodology, U.S., N.I., S.H., N.Z. and S.A.; Supervision, T.N. and S.A.; Writing—original draft, U.S., S.H., H.E. and N.Z.; Writing—review & editing, N.I. All authors have read and agreed to the published version of the manuscript.

Funding: This research received no external funding.

Acknowledgments: Research work was done at laboratories at USPCAS-E, NUST and the Department of Physical Chemistry, Quaid-e-Azam University, Islamabad, Pakistan.

Conflicts of Interest: The authors declare no conflict of interest.

References

- Pathak, S. Energy Crisis: A Review. *Int. J. Eng. Res. Appl.* **2014**, *4*, 845–851.
- Noor, T.; Ammad, M.; Zaman, N.; Iqbal, N.; Yaqoob, L.; Nasir, H. A highly efficient and stable copper BTC metal organic framework derived electrocatalyst for oxidation of methanol in DMFC application. *Catal. Lett.* **2019**, *149*, 3312–3327. [\[CrossRef\]](#)
- Shafiee, S.; Topal, E. When will fossil fuel reserves be diminished? *Energy Policy* **2009**, *37*, 181–189. [\[CrossRef\]](#)
- Qureshi, M.N. *Energy Crisis in Pakistan: A Threat to National Security*; ISSRA: Islamabad, Pakistan, 2009.
- Yaqoob, L.; Noor, T.; Iqbal, N.; Nasir, H.; Sohail, M.; Zaman, N.; Usman, M. Nanocomposites of cobalt benzene tricarboxylic acid MOF with rGO: An efficient and robust electrocatalyst for oxygen evolution reaction (OER). *Renew. Energy* **2020**. [\[CrossRef\]](#)
- Baker, B.S.; Ghezel-Ayagh, H.G. Fuel Cell System. U.S. Patents 4532192A, 30 July 1985.
- Wahab, A.; Iqbal, N.; Noor, T.; Ashraf, S.; Raza, M.A.; Ahmad, A.; Khan, U.A. Thermally reduced mesoporous manganese MOF@ reduced graphene oxide nanocomposite as bifunctional electrocatalyst for oxygen reduction and evolution. *RSC Adv.* **2020**, *10*, 27728–27742. [\[CrossRef\]](#)
- Ren, Y.; Chia, G.H.; Gao, Z. Metal–organic frameworks in fuel cell technologies. *Nano Today* **2013**, *8*, 577–597. [\[CrossRef\]](#)
- Strahl, S.; Costa-Castelló, R. Temperature control of open-cathode PEM fuel cells. *IFAC-PapersOnLine* **2017**, *50*, 11088–11093. [\[CrossRef\]](#)
- Rizvi, S.A.M.; Iqbal, N.; Haider, M.D.; Noor, T.; Anwar, R.; Hanif, S. Synthesis and Characterization of Cu-MOF Derived Cu@ AC Electrocatalyst for Oxygen Reduction Reaction in PEMFC. *Catal. Lett.* **2019**, *150*, 1397–1407. [\[CrossRef\]](#)
- Zhang, P.; Sun, F.; Xiang, Z.; Shen, Z.; Yun, J.; Cao, D. ZIF-derived in situ nitrogen-doped porous carbons as efficient metal-free electrocatalysts for oxygen reduction reaction. *Energy Environ. Sci.* **2014**, *7*, 442–450. [\[CrossRef\]](#)
- Sarwar, E.; Noor, T.; Iqbal, N.; Mehmood, Y.; Ahmed, S.; Mehek, R. Effect of Co–Ni Ratio in Graphene Based Bimetallic Electro-catalyst for Methanol Oxidation. *Fuel cells* **2018**, *18*, 189–194. [\[CrossRef\]](#)
- Wang, L.; Zhao, X.; Lu, Y.; Xu, M.; Zhang, D.; Ruoff, R.S.; Stevenson, K.J.; Goodenough, J.B. CoMn₂O₄ spinel nanoparticles grown on graphene as bifunctional catalyst for lithium–air batteries. *J. Electrochem. Soc.* **2011**, *158*, A1379–A1382. [\[CrossRef\]](#)
- Yang, W.; Salim, J.; Ma, C.; Ma, Z.; Sun, C.; Li, J.; Chen, L.; Kim, Y. Flowerlike Co₃O₄ microspheres loaded with copper nanoparticle as an efficient bifunctional catalyst for lithium–air batteries. *Electrochem. Commun.* **2013**, *28*, 13–16. [\[CrossRef\]](#)
- Jin, C.; Yang, Z.; Cao, X.; Lu, F.; Yang, R. A novel bifunctional catalyst of Ba_{0.9}Co_{0.5}Fe_{0.4}Nb_{0.1}O_{3–δ} perovskite for lithium–air battery. *Int. J. Hydrogen Energy* **2014**, *39*, 2526–2530. [\[CrossRef\]](#)
- Farrusseng, D.; Aguado, S.; Pinel, C. Metal–organic frameworks: Opportunities for catalysis. *Angew. Chem. Int. Ed.* **2009**, *48*, 7502–7513. [\[CrossRef\]](#) [\[PubMed\]](#)
- Haider, M.D.; Iqbal, N.; Rizvi, S.A.M.; Noor, T.; Hanif, S.; Anwar, R. ZIF-67 derived Cu doped electrocatalyst for oxygen reduction reaction. *J. Electrochem. Energy Convers. Storage* **2020**, *18*, 021001. [\[CrossRef\]](#)
- Xia, B.Y.; Yan, Y.; Li, N.; Wu, H.B.; Lou, X.W.D.; Wang, X. A metal–organic framework-derived bifunctional oxygen electrocatalyst. *Nat. Energy* **2016**, *1*, 15006. [\[CrossRef\]](#)
- Noor, T.; Zaman, N.; Nasir, H.; Iqbal, N.; Hussain, Z. Electro catalytic study of NiO-MOF/rGO composites for methanol oxidation reaction. *Electrochim. Acta* **2019**, *307*, 1–12. [\[CrossRef\]](#)
- Wang, R.; Dong, X.Y.; Du, J.; Zhao, J.Y.; Zang, S.Q. MOF-Derived bifunctional Cu₃P nanoparticles coated by a N, P-codoped carbon shell for hydrogen evolution and oxygen reduction. *Adv. Mater.* **2018**, *30*, 1703711. [\[CrossRef\]](#)
- Yaqoob, L.; Noor, T.; Iqbal, N.; Nasir, H.; Zaman, N. Development of nickel-BTC-MOF-derived nanocomposites with rGO towards electrocatalytic oxidation of methanol and its product analysis. *Catalysts* **2019**, *9*, 856. [\[CrossRef\]](#)
- Ghoshal, S.; Zaccarine, S.; Anderson, G.C.; Martinez, M.B.; Hurst, K.E.; Pylypenko, S.; Pivovar, B.S.; Alia, S.M. ZIF 67 Based Highly Active Electrocatalysts as Oxygen Electrodes in Water Electrolyzer. *ACS Appl. Energy Mater.* **2019**, *2*, 5568–5576. [\[CrossRef\]](#)
- Wang, H.; Wei, L.; Liu, J.; Shen, J. Hollow bimetal ZIFs derived Cu/Co/N co-coordinated ORR electrocatalyst for microbial fuel cells. *Int. J. Hydrogen Energy* **2020**, *45*, 4481–4489. [\[CrossRef\]](#)
- Yoon, H.; Lee, S.; Oh, S.; Park, H.; Choi, S.; Oh, M. Synthesis of Bimetallic Conductive 2D Metal–Organic Framework (CoxNiy-CAT) and Its Mass Production: Enhanced Electrochemical Oxygen Reduction Activity. *Small* **2019**, *15*, 1805232. [\[CrossRef\]](#)
- Wang, C.; Liu, D.; Lin, W. Metal–organic frameworks as a tunable platform for designing functional molecular materials. *J. Am. Chem. Soc.* **2013**, *135*, 13222–13234. [\[CrossRef\]](#) [\[PubMed\]](#)

26. Hanif, S.; Iqbal, N.; Shi, X.; Noor, T.; Ali, G.; Kannan, A. NiCo-N-doped carbon nanotubes based cathode catalyst for alkaline membrane fuel cell. *Renew. Energy* **2020**, *154*, 508–516. [\[CrossRef\]](#)
27. Wu, G.; Zelenay, P. Nanostructured nonprecious metal catalysts for oxygen reduction reaction. *Acc. Chem. Res.* **2013**, *46*, 1878–1889. [\[CrossRef\]](#) [\[PubMed\]](#)
28. Palaniselvam, T.; Biswal, B.P.; Banerjee, R.; Kurungot, S. Zeolitic Imidazolate Framework (ZIF)-Derived, Hollow-Core, Nitrogen-Doped Carbon Nanostructures for Oxygen-Reduction Reactions in PEFCs. *Chem. A Eur. J.* **2013**, *19*, 9335–9342. [\[CrossRef\]](#)
29. Hanif, S.; Shi, X.; Iqbal, N.; Noor, T.; Anwar, R.; Kannan, A. ZIF derived PtNiCo/NC cathode catalyst for proton exchange membrane fuel cell. *Appl. Catal. B Environ.* **2019**, *258*, 117947. [\[CrossRef\]](#)
30. Xia, W.; Zhu, J.; Guo, W.; An, L.; Xia, D.; Zou, R. Well-defined carbon polyhedrons prepared from nano metal–organic frameworks for oxygen reduction. *J. Mater. Chem. A* **2014**, *2*, 11606–11613. [\[CrossRef\]](#)
31. Aijaz, A.; Masa, J.; Rösler, C.; Xia, W.; Weide, P.; Botz, A.J.; Fischer, R.A.; Schuhmann, W.; Muhler, M. Co@Co₃O₄ encapsulated in carbon nanotube-grafted nitrogen-doped carbon polyhedra as an advanced bifunctional oxygen electrode. *Angew. Chem. Int. Ed.* **2016**, *55*, 4087–4091. [\[CrossRef\]](#) [\[PubMed\]](#)
32. Meng, F.; Zhong, H.; Bao, D.; Yan, J.; Zhang, X. In situ coupling of strung Co₄N and intertwined N–C fibers toward free-standing bifunctional cathode for robust, efficient, and flexible Zn–air batteries. *J. Am. Chem. Soc.* **2016**, *138*, 10226–10231. [\[CrossRef\]](#)
33. Ahmad, R.; Iqbal, N.; Baig, M.; Noor, T.; Ali, G.; Gul, I. ZIF-67 derived NCNT/S@Ni(OH)₂ decorated Ni foam based electrode material for high-performance supercapacitors. *Electrochem. Acta* **2020**, *364*, 137147. [\[CrossRef\]](#)
34. Yang, J.; Xu, J.J. Nanoporous amorphous manganese oxide as electrocatalyst for oxygen reduction in alkaline solutions. *Electrochem. Commun.* **2003**, *5*, 306–311. [\[CrossRef\]](#)
35. Lima, F.H.; Calegaro, M.L.; Ticianelli, E.A. Investigations of the catalytic properties of manganese oxides for the oxygen reduction reaction in alkaline media. *J. Electroanal. Chem.* **2006**, *590*, 152–160. [\[CrossRef\]](#)
36. Masa, J.; Xia, W.; Sinev, I.; Zhao, A.; Sun, Z.; Grütze, S.; Weide, P.; Muhler, M.; Schuhmann, W. Mn_xO_y/NC and Co_xO_y/NC nanoparticles embedded in a nitrogen-doped carbon matrix for high-performance bifunctional oxygen electrodes. *Angew. Chem. Int. Ed.* **2014**, *53*, 8508–8512. [\[CrossRef\]](#) [\[PubMed\]](#)
37. Liang, Y.; Wang, H.; Zhou, J.; Li, Y.; Wang, J.; Regier, T.; Dai, H. Covalent hybrid of spinel manganese–cobalt oxide and graphene as advanced oxygen reduction electrocatalysts. *J. Am. Chem. Soc.* **2012**, *134*, 3517–3523. [\[CrossRef\]](#) [\[PubMed\]](#)
38. Noor, T.; Raffi, U.; Iqbal, N.; Yaqoob, L.; Zaman, N. Kinetic evaluation and comparative study of cationic and anionic dyes adsorption on Zeolitic imidazolate frameworks based metal organic frameworks. *Mater. Res. Express* **2019**, *6*, 125088. [\[CrossRef\]](#)
39. Shi, X.; Iqbal, N.; Kunwar, S.; Wahab, G.; Kasat, H.; Kannan, A.M. PtCo@ NCNTs cathode catalyst using ZIF-67 for proton exchange membrane fuel cell. *Int. J. Hydrogen Energy* **2018**, *43*, 3520–3526. [\[CrossRef\]](#)
40. Fan, Q.; Guo, Z.; Li, Z.; Wang, Z.; Yang, L.; Chen, Q.; Liu, Z.; Wang, X. Atomic layer deposition of cobalt carbide thin films from cobalt amidinate and hydrogen plasma. *ACS Appl. Electron. Mater.* **2019**, *1*, 444–453. [\[CrossRef\]](#)
41. Yang, Z.; Wang, S.; Liu, Y.; Lei, X. Cobalt oxide microtubes with balsam pear-shaped outer surfaces as anode material for lithium ion batteries. *Ionics* **2015**, *21*, 2423–2430. [\[CrossRef\]](#)
42. Johnson, C.; Dees, D.; Mansuetto, M.; Thackeray, M.; Vissers, D.; Argyriou, D.; Loong, C.-K.; Christensen, L. Structural and electrochemical studies of α -manganese dioxide (α -MnO₂). *J. Power Sources* **1997**, *68*, 570–577. [\[CrossRef\]](#)
43. Ahmadian, H.; Veisi, H.; Karami, C.; Sedrpoushan, A.; Nouri, M.; Jamshidi, F.; Alavioon, I. Cobalt manganese oxide nanoparticles as recyclable catalyst for efficient synthesis of 2-aryl-1-arylmethyl-1H-1, 3-benzimidazoles under solvent-free conditions. *Appl. Organomet. Chem.* **2015**, *29*, 266–269. [\[CrossRef\]](#)
44. Rapson, T.D.; Kusuoka, R.; Butcher, J.; Musameh, M.; Dunn, C.J.; Church, J.S.; Warden, A.C.; Blanford, C.F.; Nakamura, N.; Sutherland, T.D. Bioinspired electrocatalysts for oxygen reduction using recombinant silk films. *J. Mater. Chem. A* **2017**, *5*, 10236–10243. [\[CrossRef\]](#)
45. Wang, W.; Geng, J.; Kuai, L.; Li, M.; Geng, B. Porous Mn₂O₃: A Low-Cost Electrocatalyst for Oxygen Reduction Reaction in Alkaline Media with Comparable Activity to Pt/C. *Chem. Eur. J.* **2016**, *22*, 9909–9913. [\[CrossRef\]](#) [\[PubMed\]](#)
46. Huang, B.; Zhang, X.; Cai, J.; Liu, W.; Lin, S. A novel MnO₂/rGO composite prepared by electrodeposition as a non-noble metal electrocatalyst for ORR. *J. Appl. Electrochem.* **2019**, *49*, 767–777. [\[CrossRef\]](#)
47. Chhetri, B.P.; Parnell, C.M.; Wayland, H.; RanguMagar, A.B.; Kannarpady, G.; Watanabe, F.; Albkuri, Y.M.; Biris, A.S.; Ghosh, A. Chitosan-derived NiO-Mn₂O₃/C nanocomposites as non-precious catalysts for enhanced oxygen reduction reaction. *ChemistrySelect* **2018**, *3*, 922–932. [\[CrossRef\]](#)
48. Atabaki, M.M.; Kovacevic, R. Graphene composites as anode materials in lithium-ion batteries. *Electron. Mater. Lett.* **2013**, *9*, 133–153. [\[CrossRef\]](#)
49. Bae, S.H.; Kim, J.E.; Randriamahazaka, H.; Moon, S.Y.; Park, J.Y.; Oh, I.K. Seamlessly conductive 3D nanoarchitecture of core-shell Ni-Co nanowire network for highly efficient oxygen evolution. *Adv. Energy Mater.* **2017**, *7*, 1601492. [\[CrossRef\]](#)
50. Lin, X. The Kinetic and Mechanism of the Oxygen Reduction Reaction on Pt, Au, Cu, PtCu/C and CuAu/C in Alkaline Media. Master's Thesis, The Ohio State University, Columbus, OH, USA, 2016.
51. Ahmad, R.; Iqbal, N.; Noor, T. Development of ZIF-Derived Nanoporous Carbon and Cobalt Sulfide-Based Electrode Material for Supercapacitor. *Materials* **2019**, *12*, 2940. [\[CrossRef\]](#)